Application of computer vision techniques for contour detection in underwater wet welding: an exploratory study

Application of computer vision techniques for contour detection in underwater wet welding: an exploratory study

J L Ortiz[1], A M Moreno-Uribe[1], B R Acevedo[2], E J Lima[1], and A R Arias[1]
[1] Robotic, Welding and Simulation Lab, Federal University of Minas Gerais, Belo Horizonte, Brazil
[2] Country Computational Intelligence Laboratory, Federal University of Minas Gerais, Belo Horizonte, Brazil

E-mail: ortizsolanojorgeluis@gmail.com

Abstract. In underwater wet welding, the process of formation and separation of the bubbles is related to the stability of the electric arc. For this reason, new methods to characterize these bubbles more quickly and accurately have become a necessity. This paper presents the application of computer vision algorithms for imaging processing to better understand the dynamics of droplets. The tests were carried out under controlled conditions that facilitate the detection and recording of the objects. The results generated by the algorithm allow in the detection and tracking of the droplets, as well as the interaction between them. The physical properties recorded were the calculation of the diameter of the drops as a function of the projected area and the average velocity of the drops.

1. Introduction

For decades, researchers have identified that in underwater wet welding, the process of formation and separation of the bubbles is related to the stability of the electric arc and consequently, to the resulting mechanical properties of the welded metal and the head affected zone (HAZ). Therefore, they have focused on a better understanding of the origin and the growth of gases between the melting pool and the tip of the electrode, considering their behavior and the dwell time of the bubbles in this area.

Masubuchi and Tsai (1977) [1] created a mathematical model to predict the growth of the bubble as an ideal gas. Subsequently, Tsai and Masubuchi (1979) [2] identified that the electric arc is always protected by the bubble during underwater welding due to the immediate vaporization of the surrounding liquid [3]. Also, a relationship has been found between the variables of the welding process and the generation of the bubbles, for example, according to de Rosa Oliveira (2012) [4], the release of the bubble may be directly related to abrupt variations of current during the underwater welding process.

Likewise, Feng, *et al*. (2017) [5] stipulate that the small diameter of the bubble is the possible factor causing its rupture, which causes the frequent extinction of the electric arc. In addition, Bernardi (2018) [6], states that, the higher the welding current, the greater the stability of the arc and the greater the average diameter of the bubbles, this is related to a higher melting rate of the consumable and to a greater repeatability of the experiments. This trend remains undifferentiated with the polarity of the welding current.

Mendonça and Bracarense (2019) [7] evidenced that the formation of the bubbles is closely related to the variation of the electrical signals and the stability of the electric arc. In addition, they concluded that, through the adjustment of the parameters of the welding process, it is possible to optimize the

diameter of the bubble and the frequency of its formation to obtain more stable electric arcs during welding.

Just as Bernardi (2018) [6], and Mendonça and Bracarense (2019) [7] studied the stability of the electric arc by analyzing the variation of the size of the bubbles as a function of the variation of traditional welding parameters, other authors have chosen to study different alternatives to understand this process. Wu, *et al*. (2020) [8], modified the welding current with the aim of controlling the detachment of the bubbles, Zhao, *et al*. (2020) [9] simulated the generation and behavior of the bubble using hydrodynamics, and Wang, *et al*. (2018) [10] used an assisted mechanical constraint to retain the bubble, protecting the welding arc for longer.

With the studies already mentioned and considering the important role played by the permanence of the bubble in the melting pool on the stability of the process, it is concluded that the application of methodologies of characterization of underwater wet welding such as, for example, techniques of visual study (through images), have become highlighted in recent years.

Thus, this work is a study of the application of computer vision algorithms for image processing, with the aim of understanding the dynamics of the bubbles and of ease the research of a relation between this dynamic and a better performance of the welding union. Currently, no computer vision applications have been performed in underwater wet welding due to the interference of the electric arc in the image.

This created the need for a preliminary test under controlled conditions to facilitate the process of detection and registration of the physical properties like the area and the velocity of the studied objects when characterizing a process that involves plasma and the electric arc. In order to do so, the algorithm uses open-source computer vision library (OpenCV) [11], which is an open-source library for image and video analysis, for the pre-processing of the images, the detection of the contour of the objects and the determination of the area projected by the drops when they are sprayed. In addition, the algorithm keeps track of the droplets, calculate their average velocity and detects interactions between them like fusion or separation.

2. Proposed methodology

For these experiments, the technique of high-speed photography was used with a camera Phantom model 2512, Vision Research and a light-emitting diode (LED) of 7,000 lumens on the back (directed towards the camera). In the process, the drops coming out of a manually operated spray bottle at 25,000 frames per second were filmed.

The procedure for the detection, the measure of physical properties (area and velocity) and the tracking of the objects in the video is shown in Figure 1. Initially, with the equipment described above there were filmed video with high contrast between the objects and the background to facilitate the detection (see Figure 1(a)). Then, image per image (frames) were extracted from the video. Subsequently, a workspace was established, represented by a 581×886 pixel window located in the area of interest (Figure 1(a)). Afterward, the preprocessing of the image, the edges extraction and the calculation of variables were carried out.

With the selected window (see Figure 1(a)), the preprocessing of the image was carried out (see from Figure 1(b) to Figure 1(d)). First, the image was binarized (see Figure 1(b)) using an adaptive threshold with a neighborhood of 11 pixels. Also, morphological operators such as the dilation of 2 iterations with a 3×3 kernel were applied to close the contours of the detected objects. Then, the imfill (Fill image regions and holes) function (as defined by Kalakuntla and Andriamanalimanana (2020) [12]) was applied, which consists of filling the closed contours (see Figure 1(c)). Finally, as showed in Figure 1(d), the image underwent an opening (an erosion followed by an expansion) of 4 iterations and an erosion with a 5×5 kernel to eliminate the noise resulting from previous operations.

To find the contour of the objects in the preprocessed image, the programing function findContours available in the OpenCV library was arbitrarily applied (see Figure 1(e)), and then, use these contours to calculate the centroid and the projected area (in pixels) for each object.

This algorithm locates the centroid of each droplet and stores it together with its respective frame in a python dictionary. Within the dictionary is also stored the projected area (in pixels), which is used to

calculate the equivalent diameter of the droplets. The Equation (1) was used to compute the mentioned diameter [13].

$$d = \left(\frac{4*A}{\pi}\right)^{1/2}, \quad (1)$$

where A is the projected area and d is the diameter (in pixels); with the position of the centroid and the area of each element the smallest distance between centroids was used to identify each drop independently, and thus execute a tracking of them through the frames. Also, taking into account the frames and the frame rate, the time was estimated, and it proceeded to calculate the speed of the drops.

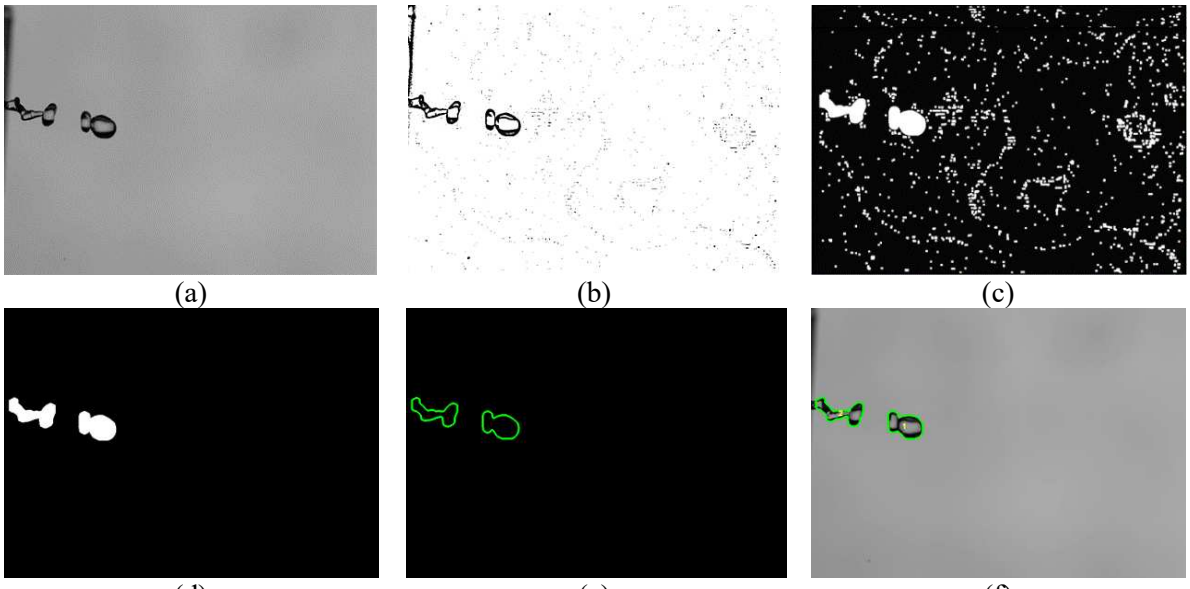

Figure 1. The proposed methodology; (a) the window of interest of the image (581 x 886 pixels); (b) the result of applying an adaptive thresholding (mean); (c) the Imfill function to fill the closed contours; (d) an opening morphological transformation (an erosion followed by a dilation) and an erosion applied; (e) the extracted edges of the resulting objects; (f) the labeled of the objects.

3. Results and discussions

Analyzing the video and the behavior of the drops, it was documented that there are unions and separations between them. Which generated the need to define how the algorithm was going to monitor the drops under those circumstances. Thus, the following was defined. On the separation of an object, the one that projects a larger area maintains the label of the previous object; and the smaller object gets a new label. In a union of two objects, the smaller loses its label, and consequently its monitoring. Therefore, the largest object continues to be monitored with the same label.

It was also found that the drops took a three-dimensional direction while it was a two-dimensional were sensed (camera). This allowed to identify that some behaviors could be misinterpreted, and this would lead to errors in the results. For example, it could not be easily identified if the displacement of the droplet moved it away or closer to the camera as the variation in the projected area is negligible. In the same way, if a drop passes with a different depth from another with respect to the camera but in the same sensing plane, the projection of its areas will overlap, and the algorithm could not perceive that there was no union between the two. In this case, it is possible that an error was made both by detecting a false union of these drops and by detecting their subsequent separation. This because the probability that the component of the direction of the two drops were the same is very low.

That said, the results are presented as follows. First, the displacement in the horizontal (see Figure 2) and the vertical (see Figure 3) axes of the bodies of water with better behavior are presented. The horizontal displacement is linear (first order) for the majority, and, in the vertical component, as expected, there is a second order (parabolic) movement. In those images it can be seen unusual variations in the displacement of the centroid of some drops in time, for example, drop 10 and drop 12 joins in the frame 1210 (see Figure 2, black circle) and due to the defined union criterion, the algorithm continues to monitor this new object with the label number 10.

Another example of this can be seen in Figure 2, where in frame 980 (see Figure 2, red circle) drop 7 and drop 11 joined, and, from there, only the 11 was monitored. Another example occurred in the frame 970 (see Figure 3, black circle) when the objects labeled as 3 and 6 become a single body with drop 4. A particular case is evidenced in Figure 3, the displacement of the drop 5, where immediately after the formation of drop 8, the areas of drop 8 and drop 5 are superimposed in the frame 810 and their projected areas are separated in the frame 970, this makes that erroneously the algorithm interprets them as a union where the drop 5 maintains its label in the monitoring and when they move away in the plane of vision of the camera, the sudden movement of the displacement of the centroid of this object can be perceived.

Second, Figure 4 shows a typical behavior of the size in pixels of the equivalent diameter projected by a body of water through the frames. The variation of the area is due to the dynamics of the expelled drop that depends on the atmospheric conditions of the environment and the pressure exerted by the person to the embolus of the spray bottle.

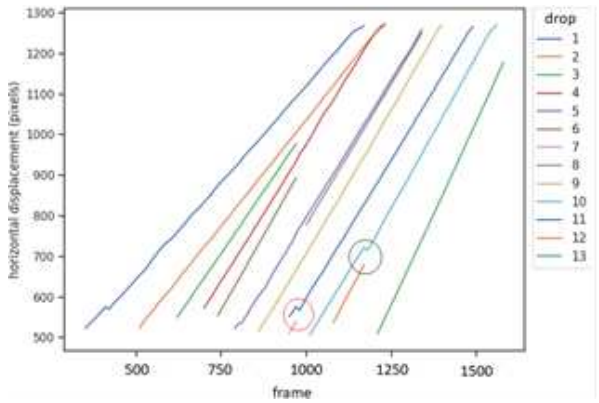

Figure 2. Horizontal displacement of the drops.

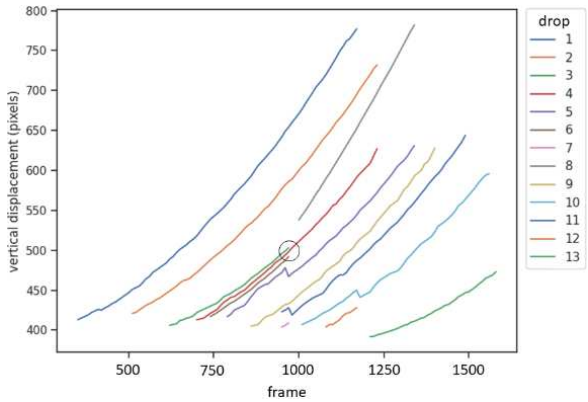

Figure 3. Vertical displacement of the drops.

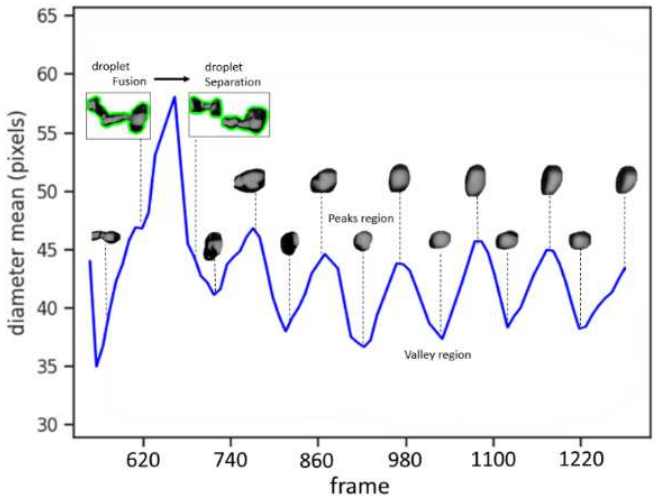

Figure 4. Equivalent diameter projected by a drop over time.

The drop comes out of the spray in an elongated form. However, this process is transient, and, after the detachment from the spray, it behaves, as mentioned by Svintradze [14], like an elastic ball where its dynamics fluctuate in a steady-state behavior until it leaves the image.

Third, the diameters and the average velocities of the droplets are presented. Figure 5 shows the equivalent average of the projected areas of each drop in pixels and Figure 6 illustrates the average velocity, which is affected by the dynamics of these objects. The drops with higher diameter, and then higher volume, are likely to have a smaller average velocity.

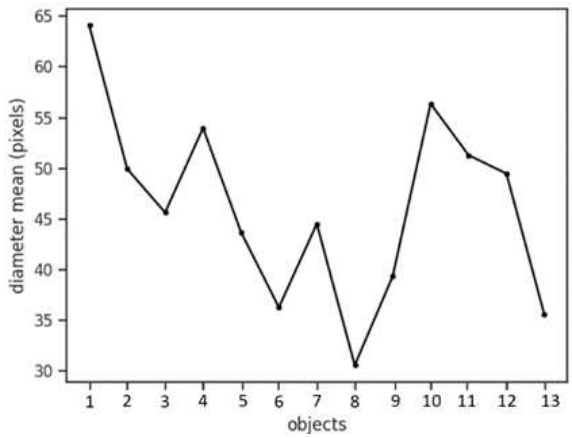

Figure 5. Mean of the equivalent diameter of each drop in pixels.

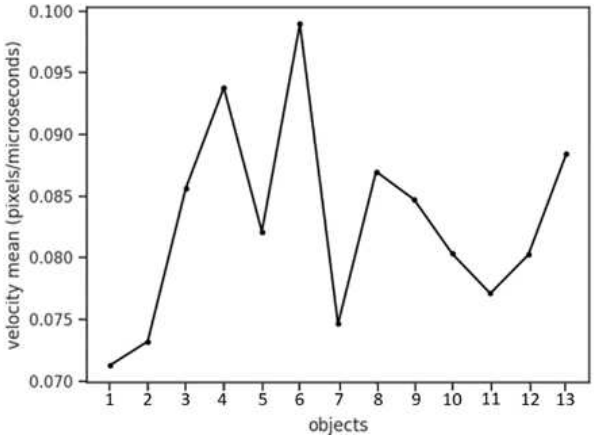

Figure 6. Average speed of each drop in pixels/microseconds.

4. Conclusions

The results generated by the algorithm allowed the detection and tracking of the droplets, as well as a better understanding of the interaction between them.

The study by calculating the projected area and the centroid of this area facilitated their tracking and the study of motion in more than one dimension; despite the limitations in the differentiation of two intersecting bodies, the precision of the areas projected in the images allows a better study of the behavior of these droplets over time. The results are sufficient to proceed to the study of the phenomenon of bubble formation during the wet underwater welding process.

Acknowledgments

The authors would like to acknowledge and thank DVPRO Engenharia de televisão and Vision Research Inc. for their fundamental contribution in the creation of the video. This work was supported by the national research center CNPq (Grant number 132092/2020-4).

References

[1] Masubuchi K, Tsai C L 1977 *Welding Research Council Bulletin: Interpretive Report on Underwater Welding* (New York: The Welding Research Council)

[2] Tsai C L, Masubuchi K 1980 Mechanisms of rapid cooling and their design considerations in underwater welding *J. Pet. Technol* **32(10)** 1825

[3] Pope A M, De Medeiros R C, Liu S 1995 Solidification of underwater wet welds *International Conference on Offshore Mechanics and Arctic Engineering* (Copenhagen: American Society of Mechanical Engineers, Offshore Mechanics and Arctic Engineering Division)

[4] De Rosa Oliveira F 2012 *Estudo Sobre o Correlacionamento do Fenômeno das Bolhas, Sinais Elétricos e Metal de Solda na Soldagem Subaquática Molhada com Eletrodos Revestidos* (Belo Horizonte: Universidade Federal de Minas Gerais)

[5] Feng J, Wang J, Sun Q, Zhao H, Wu L, Xu P 2017 Investigation on dynamic behaviors of bubble evolution in underwater wet flux-cored arc welding *Journal of Manufacturing Processes* **28(1)** 156

[6] Bernardi R A 2018 *Investigações de Ordem Operacional e Implementação de Tecnologias para Soldagem Subaquática Molhada com Eletrodos Revestidos* (Florianópolis: Universidade Federal de Santa Catarina)

[7] Mendonça C M, Bracarense A Q 2019 Investigação do fenômeno das bolhas em soldagem subaquática molhada com arame tubular autoprotegido *Soldagem & Inspeção* **24** e2416
[8] Wu J, Han Y, Jia C, Wu C, Yang Q 2020 Underwater pulse-current FCAW Part 2: Bubble behaviors and waveform optimization *Welding Journal* **99(12)** 303-s
[9] Zhao B, Chen J, Wu C, Shi L 2020 Numerical simulation of bubble and arc dynamics during underwater wet flux-cored arc welding *Journal of Manufacturing Processes* **59** 167
[10] Wang J, Sun Q, Zhang S, Wang C, Wu L, Feng J 2018 Characterization of the underwater welding arc bubble through a visual sensing method *Journal of Materials Processing Technology* **251** 95
[11] Culjak I, Abram D, Pribanic T, Dzapo H, Cifrek M 2012 A brief introduction to OpenCV *International Convention MIPRO* (Opatija: Croatian Society for Information, Communication and Electronic Technology)
[12] Kalakuntla S, Andriamanalimanana B R 2020 *Detection of Brain Tumor in Magnetic Resonance Imaging (MRI) Images Using Fuzzy C-Means and Thresholding* (Utica: State University Of New York Polytechnic Institute)
[13] Araújo D B, Vilarinho L O, Resende A A 2011 Investigação da transferência metálica por meio do processamento digital de imagem *6° Congresso Brasileiro de Engenharia de Fabricação* (Caxias do Sul: Associação Brasileira de Engenharia e Ciências Mecânicas)
[14] Svintradze D V 2019 Shape dynamics of bouncing droplets *Scientific Reports* **9(1)** 6105